GSA Data Repository item 2019218

Overestimation of threat from 100 Mt-class airbursts?

high-pressure evidence from zircon in Libyan desert glass

Aaron J. Cavosie[1] and Christian Koeberl[2,3]

[1]*Space Science and Technology Centre and The Institute for Geoscience Research (TIGeR), School of Earth and Planetary Science, Curtin University, Perth, WA 6102, Australia*
[2]*Natural History Museum, Burgring 7, A-1010 Vienna, Austria*

[3]*Department of Lithospheric Research, University of Vienna, Althanstrase 14, A-1090 Vienna, Austria*

Contents

Item DR1. Additional information on samples.

Sample name, location information, and representative optical images.
The seven Libyan Desert Glass (LDG) samples analyzed in this study were collected in Egypt by Christian Koeberl, and are labeled as follows:

Sample name:
(1) LDG-2018-1 (Lok.1)
(2) LDG-2018-2
(3) LDG-2018-3
(4) LDG-2018-4
(5) LDG-2018-5
(6) LDG-2018-6
(7) LDG-2018-ZE-1

The camp was located on the eastern flank of a large sand dune, which is continually changing position. The coordinates of the camp are approximately N25° 28.23' and E25°32.28'. All of the samples were found within a few hundred meters of the camp. The samples were collected from lag deposits between dunes.

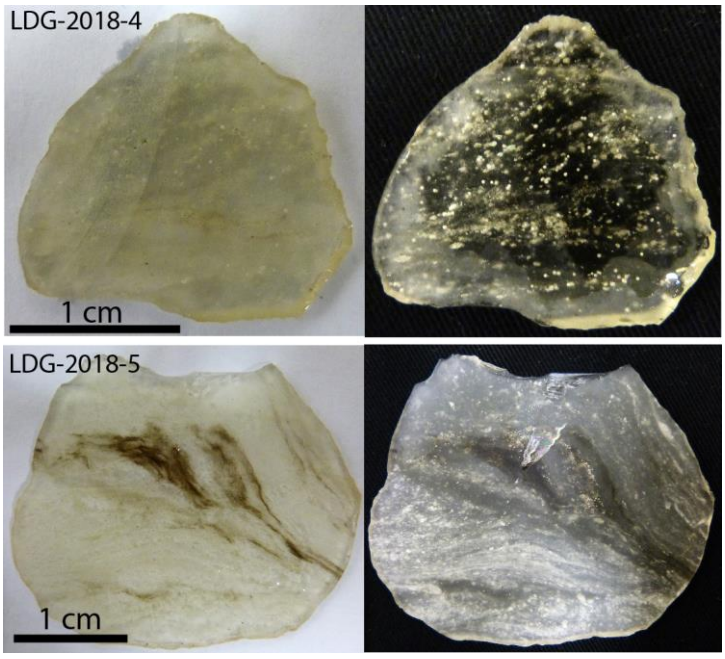

Figure DR1. Optical light images with a light background (left) and dark background (right) of representative LDG samples analyzed in this study. The zircons shown in Figure 2 of the main manuscript, Figure DR2A, Figure DR6, and Figure DR7 are all from sample LDG-2018-4 (top image).

Item DR1 (cont.).
Representative BSE images of zircon grains in LDG.

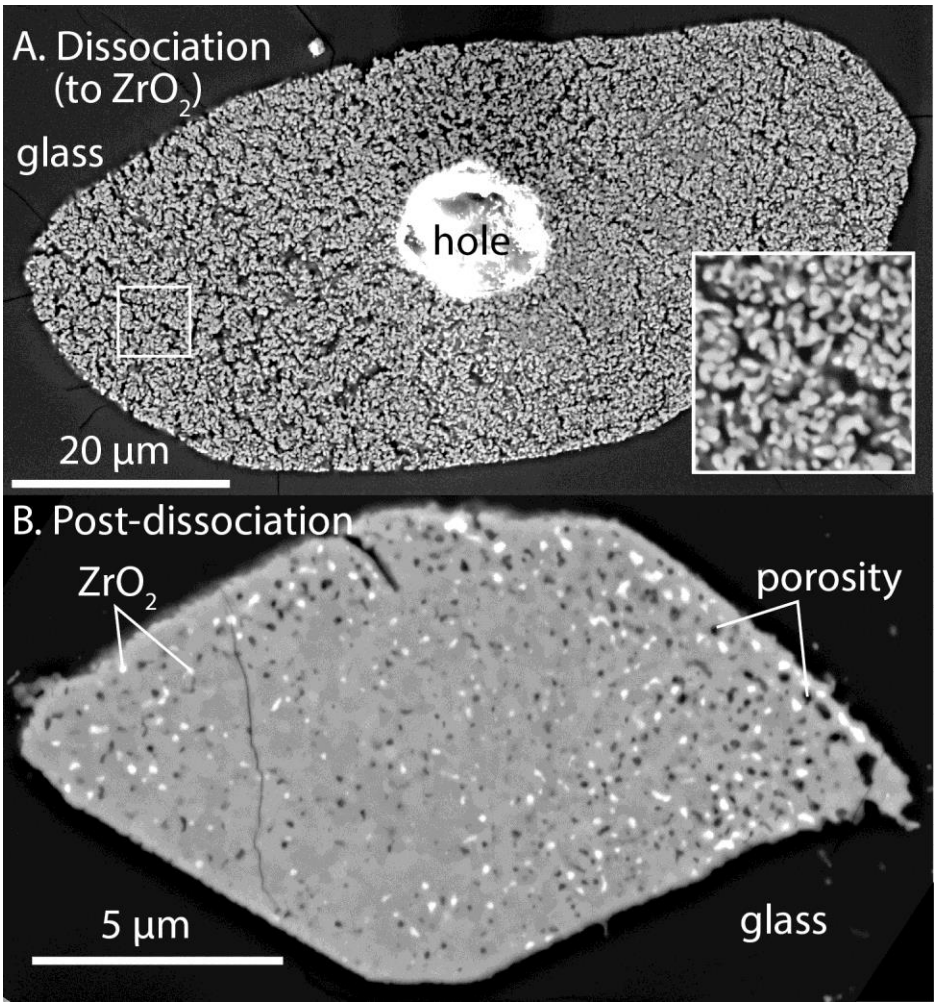

Figure DR2. BSE images of zircon grains in LDG. **A**: Zircon grain that dissociated to zirconia (baddeleyite), sample LDG-2018-4. **B**: Zircon grain that is interpreted to have dissociated to zirconia, and then back-reacted with melt to form neoblastic zircon (referred to as nz2 in the main text), sample LDG-2018-2.

Item DR1 (cont.).
Additional images of the zircon shown in Figure 2 (LDG-2018-4, grain 1).

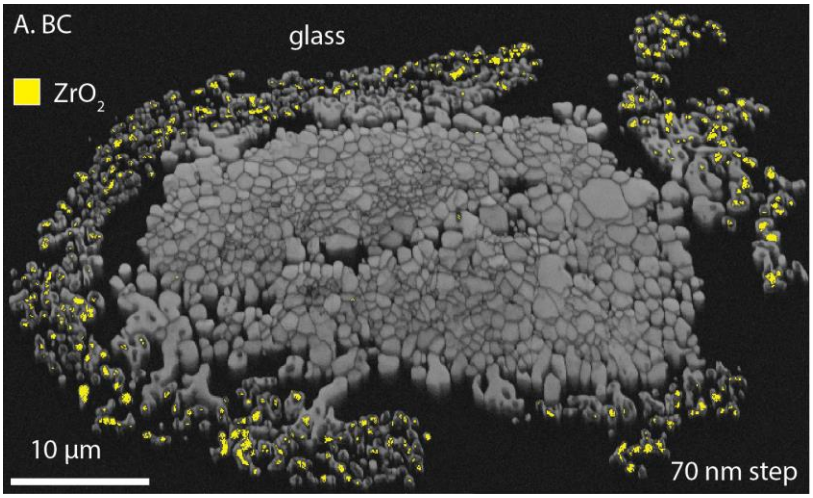

Figure DR3. Combined band contrast (BC) and phase color image. The neoblastic texture of the core of the zircon, including sharp grain boundaries between neoblasts, is readily visible. The presence of baddeleyite (ZrO_2) is shown in yellow, and is primarily located in the semi-detached rim.

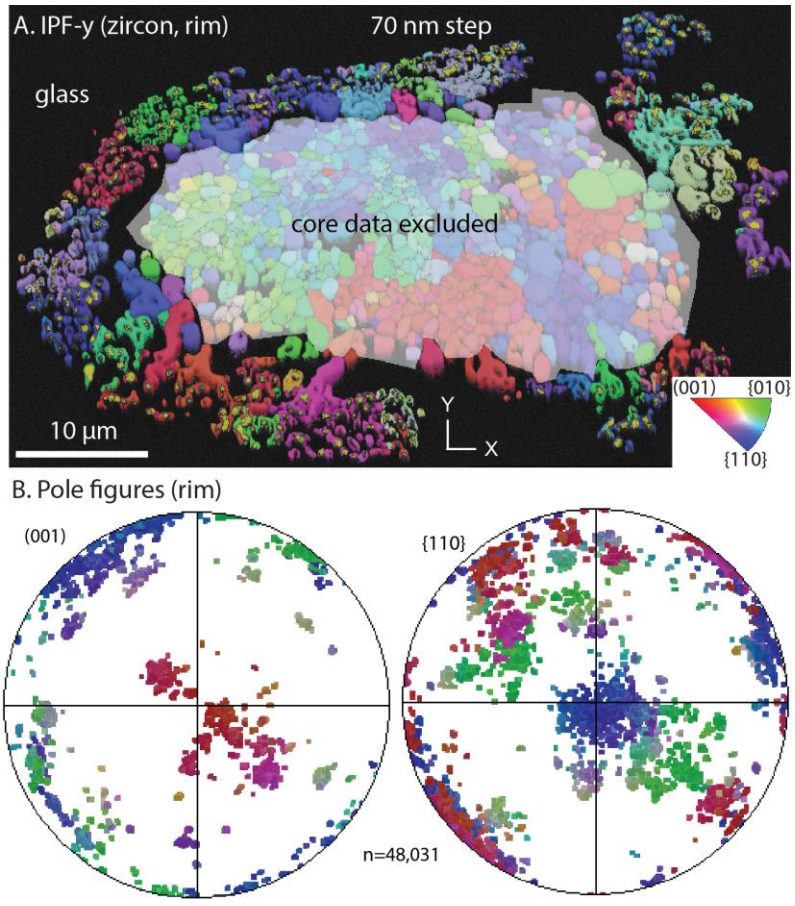

Figure DR4. Orientation map (inverse pole figure color scheme) showing zircon data for the semi-detached rim only (data from the neoblastic core were excluded). The rim is comprised of at least 15 orientation clusters, whereas the core is comprised of 3. While a few of the rim clusters are in similar orientations to the core, most are tightly clustered and do not overlap with the core orientations (note color variation).

Item DR1 (cont.).
Additional images of the zircon shown in Figure 2 (LDG-2018-4, grain 1).

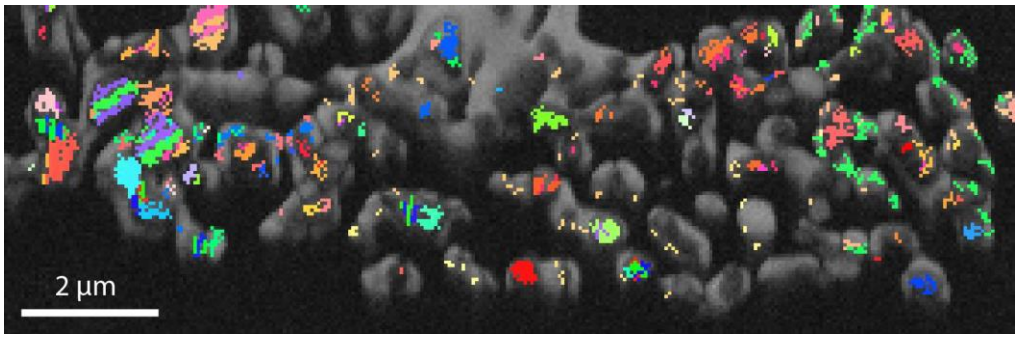

Figure DR5. Orientation map (Euler coloring scheme) showing pervasive twinning in baddeleyite grains from the rim, which records reversion from tetragonal zirconia. The location of this map in the rim is in the center, and at the bottom, of **Figure DR3**. Step size is 50 nm.

Representative example of a granular zircon that preserves evidence of former reidite.

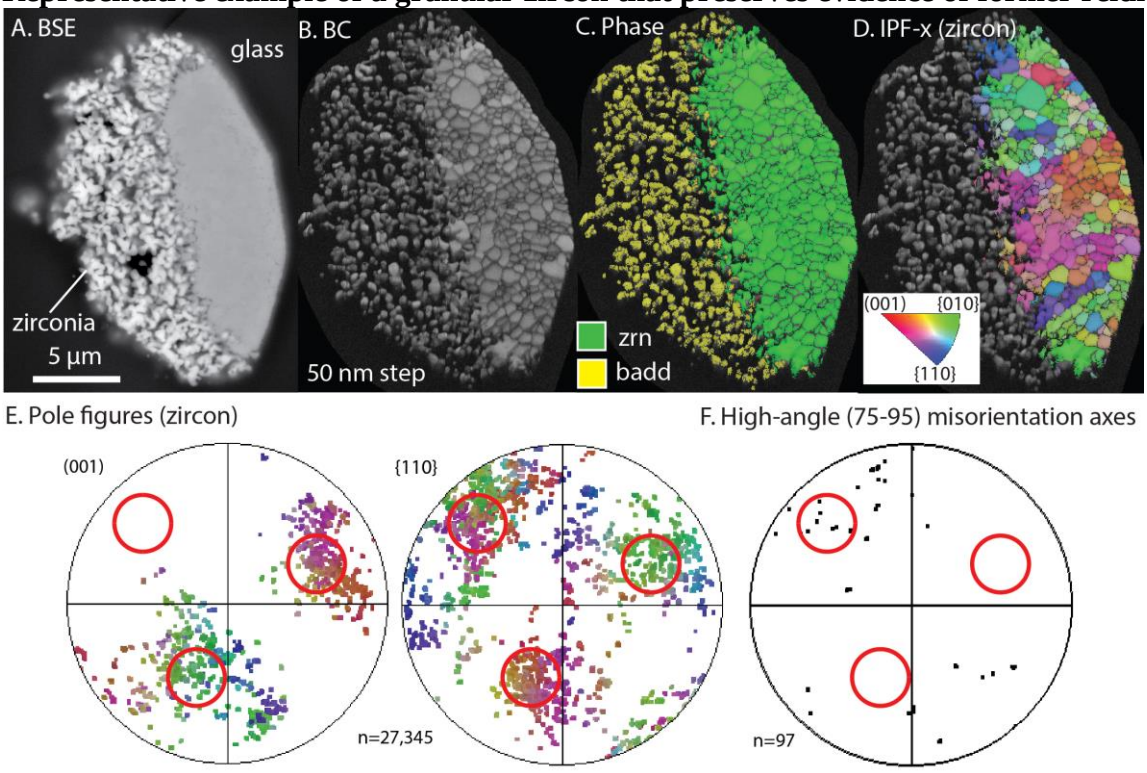

Figure DR6. Granular zircon that preserves evidence of former reidite (sample LDG-2018-4b, grain 5). **A**: BSE image, showing partial dissociation. Note preserved prism and pyramid faces. **B**: Band contrast (BC) image, showing boundaries between zircon neoblasts. **C**: Phase map (zircon is green, baddeleyite is yellow). **D**: Orientation map with an inverse pole figure (IPF-x) color scheme. **E**: Pole figures, showing two orientation clusters (001), that coincide with <110> directions. **F**: High-angle misorientation axis distribution, showing overlap with one <110> direction. Red circles show locations of predicted 90°/<110> orientation relations based on data in the (001) pole figure. One red circle contains no data [see (001)], as only one orientation of reidite was originally present.

Item DR1 (cont.).
Representative example of a granular zircon that does not preserve evidence of former reidite.

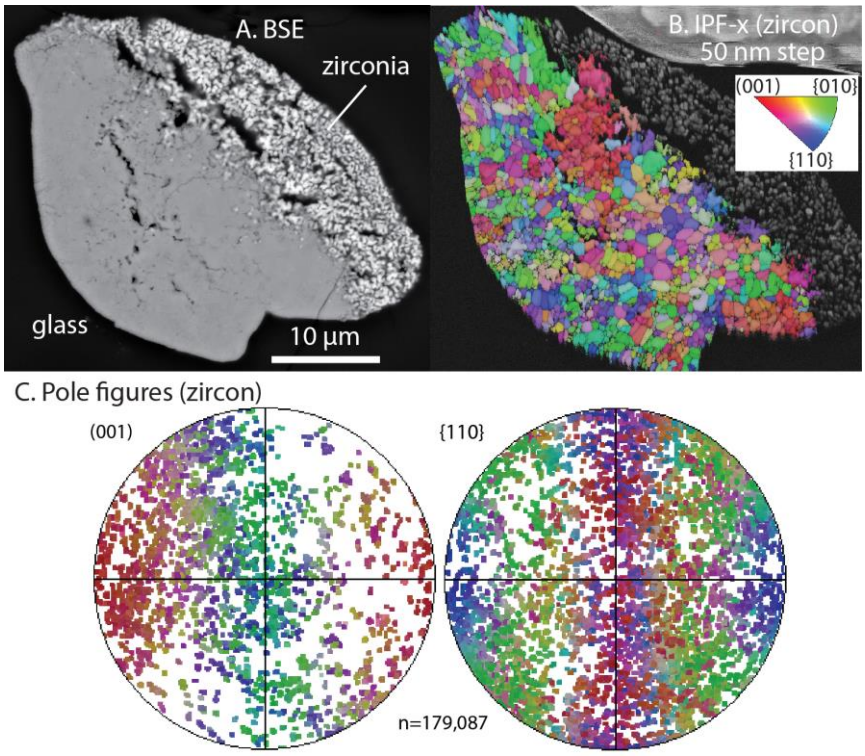

Figure DR7. Representative example of a granular neoblastic zircon in LDG (sample LDG-2018-5, grain 27) that does not preserve neoblast orientation clusters indicative of reidite. **A**: BSE image, showing that the margin of the grain has dissociated to zirconia. **B**: Orientation map with an inverse pole figure color scheme. C: Pole figures showing broadly dispersed orientations, with no discrete orientation clusters.

Item DR2. Additional information on methods.

Scanning electron microscopy (SEM) analysis was done using a Tescan MIRA3 field emission gun (FEG) SEM in the Microscopy and Microanalysis Facility in the John de Laeter Centre at Curtin University. The FEG-SEM was used for BSE, energy dispersive spectroscopy (EDS), and electron backscatter diffraction (EBSD). EBSD maps were made by indexing electron backscatter diffraction patterns on areas of interest. Maps were collected using step sizes of 50 to 100 nm. EBSD analyses were collected with a 20 kV accelerating voltage, 70° sample tilt, 20.5 mm working distance, and 18 nA beam intensity. Electron backscatter patterns were collected with a Nordlys Nano high-resolution detector and Oxford Instruments Aztec system using routine data acquisition and noise reduction settings (Table DR1; see examples of recent method descriptions and applications to granular zircon in Cavosie et al., 2018a,b). EBSD maps and pole figures were processed using the Tango and Mambo modules in the Oxford Instruments/HKL Channel 5 software package version 5.12; misorientation plots were made using version 5.11. Full EBSD analysis conditions are listed in Table DR1. Each EBSD map included match units for zircon (zircon5260, Mincryst database card 5260, 1 atm; Hazen and Finger, 1979, reidite (Reidite6032, 0.69 GPa; Farnan et al., 2003), and baddeleyite (monoclinic ZrO_2; Bondars et al., 1995).

The EBSD map shown in Figure 2B is an inverse pole figure map, which is color-coded to show orientation as a function of crystallography (Miller index). Pole figures for relevant planes in zircon (e.g., (001) and {110}) were plotted as lower hemisphere equal area plots with the same x-y-z reference frame as the EBSD maps (Figs. 2C).

The Mambo software module calculates misorientation axes based on neighbor pairs, and misorientation axis orientations were calculated for misorientation angles from 75° to 95°, those that correspond to the characteristic 90°/<110> misorientation associated with reidite. Misorientation axes were plotted as lower hemisphere, equal area plots in the x-y-z reference frame of the EBSD maps (Fig. 2D).

REFERENCES CITED IN THE DATA REPOSITORY

Bondars, B., Heidemane, G., Grabis, J., Laschke, K., Boysen, H., Schneider, J., and Frey, F., 1995, Powder diffraction investigations of plasma sprayed zirconia: Journal of Materials Science, v. 30, p. 1621–1625.

Cavosie, A.J., Timms, N.E., Ferrière, L, and Rochette, P., 2018a, FRIGN zircon- The only terrestrial mineral diagnostic of high-pressure and high-temperature shock deformation: Geology, v. 46, p. 891–894, https://doi.org/10.1130/G45079.1.

Cavosie, A.J., Timms, N.E., Erickson, T.M., and Koeberl, C., 2018b, New clues from Earth's most elusive impact crater: Evidence of reidite in Australasian tektites from Thailand: Geology, v. 46, p. 203-206.

Farnan, I., Balan, E., Pickard, C.J., and Mauri, F., 2003, The effect of radiation damage on local structure in the crystalline fraction of $ZrSiO_4$: investigating the ^{29}Si NMR response to pressure in zircon and reidite: American Mineralogist, v. 88, p. 1663-1667.

Hazen, R.M., and Finger, L.W., 1979, Crystal structure and compressibility of zircon at high pressure: American Mineralogist, v. 64, p. 196–201.

Table DR1. EBSD analysis conditions.

Sample: LDG-2018-4	04a-1	04a-1	04bS1-5	04bS2-27
Whole grain (WG) or region of interest (ROI)	WG	ROI	WG	WG
Show in figure	2B	DR	DR	DR
Systematic zircon neoblast orientations	yes	-	yes	no
Acquisition speed (Hz)	40	40	40	40
Background (frames)	64	64	64	64
Binning	4 x 4	4 x 4	4 x 4	4 x 4
Gain	High	High	High	High
Hough resolution	60	60	60	60
Band detection (min)	12	12	12	12
Mean angular deviation (zircon)	0.60	-	0.56	0.48
Mean angular deviation (baddeleyite)	0.70	0.72	0.67	0.63
X steps	804	294	284	750
Y steps	532	101	418	614
Step distance (nm)	70	50	50	50
Noise reduction methods				
Wildspike	yes	yes	yes	yes

SEM Model: Tescan Mira3 FEG-SEM, Curtin Univ.
EBSD system: Nordlys Detector- Aztec
Match units for the above maps: Zircon5260; ZrO2 monoclinic
All grain are in chips of Libyan desert glass.
The LDG chips are mounted in epoxy.
The samples were coated with a thin (<5 nm) carbon coat,
mounted flat, and grounded with Cu tape.
The samples were rotated to a 70° tilt by moving the stage.
The accelerating voltage was 20 kV, and the
working distance was ~20.5 mm for all analyses.